Computer Studies of the Slowing Down of Energetic Atoms in Crystals

MARK T. ROBINSON AND ORDEAN S. OEN
Solid State Division, Oak Ridge National Laboratory, Oak Ridge, Tennessee*
(Received 29 July 1963)

The slowing down of 1- to 10-keV Cu atoms in fcc, bcc, and diamond-structure crystals has been investigated by high-speed digital computer techniques, using exponentially screened Coulomb and Born-Mayer potentials to describe the interatomic repulsion. The ranges of these atoms prove to be strongly dependent on their initial directions of motion, the order of ranges being

fcc	[011]>[001]>[111]≈isotropic,
bcc	[111]>[001]>[011]>isotropic,
diamond	[011]>[001]≈[111]>isotropic.

This orientation dependence of the range, which has also been observed experimentally, is a consequence of the tendency of the lattice to focus moving particles into channels bordered by relatively closely packed atomic rows. Inclusion of zero-point vibrations reduces the degree of channeling, but does not modify the order of ranges for fcc. The experimental evidence for channeling and some of its implications for radiation damage theory are discussed.

I. INTRODUCTION

UNTIL very recently, it has been assumed in most experimental[1–3] and theoretical[4–7] studies that the slowing down of energetic atoms in crystals is little influenced by lattice correlations, at least as long as energies greater than a few hundred eV are considered. As such atoms slow down, they suffer occasional major changes of direction due to close encounters with lattice atoms, and it has been argued[7] that these large angle scatterings smear out any lattice effects which might otherwise obtain, in spite of the fact that visual examination of "stick-and-ball" crystal models suggests that atoms might penetrate more readily in some crystallographic directions than in others.[8,9] Our recently reported computer studies[7] of the ranges of energetic atoms were based on a randomized model of a solid in which only its density was preserved, no account being taken of the directional properties of the lattice. These calculations produced results in generally good agreement with experiment,[1–3] at least considering the uncertainty of the interatomic potential. The most striking failure of the random model, however, was its inability to explain the strongly penetrating component observed by Davies and his co-workers[3] for several ions slowing down in polycrystalline aluminum and tungsten. On the basis of a new model, in which the atoms of the solid are correctly located on lattice sites, we have recently interpreted this penetrating component as a consequence of the channeling of the energetic primaries in certain preferred crystallographic directions.[10] These same calculations predicted that the penetrations of atoms into monocrystalline targets would depend rather sensitively on the crystallographic orientation of the incident beam, a prediction which has now been confirmed experimentally for 40-keV $^{85}Kr^{+}$ ions slowing down in monocrystalline aluminum.[11] The penetrating component for the same ions in polycrystalline tungsten has also been shown to be due to a lattice effect.[12]

Before entering upon a description of the model, it is appropriate to indicate something of the philosophy underlying the calculations, in order that both their value and their limitations may be appreciated. Machine computations of the sort described here partake very

* Oak Ridge National Laboratory is operated by Union Carbide Corporation for the U. S. Atomic Energy Commission.

[1] R. A. Schmitt and R. A. Sharp, Phys. Rev. Letters **1**, 445 (1958); V. A. J. van Lint, R. A. Schmitt, and C. S. Suffredini, Phys. Rev. **121**, 1457 (1961).

[2] D. Powers and W. Whaling, Phys. Rev. **126**, 61 (1962).

[3] J. A. Davies, J. Friesen, and J. D. McIntyre, Can. J. Chem. **38**, 1526 (1960); J. A. Davies, J. D. McIntyre, R. L. Cushing, and M. Lounsbury, *ibid.* **38**, 1535 (1960); J. A. Davies and G. A. Sims, *ibid.* **39**, 601 (1961); J. A. Davies, J. D. McIntyre, and G. A. Sims, *ibid.* **40**, 1605 (1962); I. Bergström, F. Brown, J. A. Davies, J. S. Geiger, R. L. Graham, and R. Kelley, Nucl. Instr. Methods **21**, 249 (1963); J. A. Davies, B. Domeij, and J. Uhler, Ark. Fys. **24**, 377 (1963); I. Bergström, J. A. Davies, B. Domeij, and J. Uhler, *ibid.* **24**, 389 (1963); B. Domeij, I. Bergström, J. A. Davies, and J. Uhler, *ibid.* **24**, 399 (1963); J. Uhler, B. Domeij, and S. Borg, *ibid.* **24**, 413 (1963); J. A. Davies, F. Brown, and M. McCargo, Can. J. Phys. **41**, 829 (1963); F. Brown and J. A. Davies, *ibid.* **41**, 844 (1963); M. McCargo, F. Brown, and J. A. Davies, Can. J. Chem. **41**, 2309 (1963).

[4] K. O. Nielsen, in *Electromagnetically Enriched Isotopes and Mass Spectrometry* (Academic Press Inc., New York, 1956), p. 68.

[5] D. K. Holmes and G. Leibfried, J. Appl. Phys. **31**, 1046 (1960); J. Lindhard and M. Scharff, Phys. Rev. **124**, 138 (1961); G. Leibfried, J. Appl. Phys. **33**, 1933 (1962); G. Leibfried, Z. Physik **171**, 1 (1963).

[6] V. A. J. van Lint and M. E. Wyatt, Jr., U. S. Air Force Report ARL 62-389, June 1962 (unpublished).

[7] M. T. Robinson, D. K. Holmes, and O. S. Oen, in *Le Bombardement Ionique* (Centre National de la Recherche Scientifique, Paris, 1962), p. 105; O. S. Oen, D. K. Holmes, and M. T. Robinson, J. Appl. Phys. **34**, 302 (1963); O. S. Oen and M. T. Robinson, Bull. Am. Phys. Soc. **8**, 195 (1963).

[8] G. J. Ogilvie, J. Phys. Chem. Solids **10**, 222 (1959).

[9] A. L. Southern, W. R. Willis, and M. T. Robinson, J. Appl. Phys. **34**, 153 (1963); J. M. Fluit, P. K. Rol, and J. Kistemaker, *ibid.* **34**, 690 (1963).

[10] M. T. Robinson and O. S. Oen, Appl. Phys. Letters **2**, 30 (1963); Bull. Am. Phys. Soc. **8**, 195 (1963); M. T. Robinson, D. K. Holmes, and O. S. Oen, Bull. Am. Phys. Soc. **7**, 170 (1962).

[11] G. R. Piercy, J. A. Davies, M. McCargo, and F. Brown, Bull. Am. Phys. Soc. **8**, 196 (1963); G. R. Piercy, F. Brown, J. A. Davies, and M. McCargo, Phys. Rev. Letters **10**, 399 (1963).

[12] M. McCargo, J. A. Davies, and F. Brown, Can. J. Phys. **41**, 1231 (1963).

largely of the nature of experiments: Not only are they subject to statistical uncertainties, but also they must be understood inductively. The present model has proved to be extremely sensitive to what were initially thought to be minor details, to an extent which presently precludes *quantitative* comparison with experiments. Consequently, it has seemed appropriate to emphasize primarily the *qualitative* behavior of the model, particularly those aspects which can be tested experimentally. To this end, the particular emphasis of this communication will be on a discussion of the model and of the influence of lattice symmetry on the results of our calculations.

II. BASIS OF THE MACHINE CALCULATIONS

A. Description of the Model

The model on which the present calculations are based is essentially similar to that employed in our earlier work,[7] except that the atoms of the target crystal are now correctly located on lattice sites. As in the earlier calculations, the primary atom is assumed to slow down over a preset energy range by means of classical binary elastic collisions with the atoms of the target crystal. Interactions of the target atoms with each other are ignored. In order to ensure that principally two-body interactions occur, the interatomic potential is assumed to have a finite range, outside of which it vanishes. The consequences of this are discussed in Sec. IIB.

The computer, an IBM 7090, proceeds from one collision to the next by searching the lattice for an appropriately located target atom. The "free-flight" distance, introduced into our random model[7] to preserve the solid density, is unnecessary and, in fact, the value used in the earlier work may be tested by comparison with the present calculation. Although the calculations which have been performed are restricted to cubic crystals, the program is designed to handle orthorhombic crystals with several nonequivalent atoms. If the primary is moving precisely in certain crystallographic directions, and if the range of the potential is such that the target atoms overlap, the primary may properly be required to interact simultaneously with two (or more) target atoms. The program will generally treat this situation as the superposition of two independent collisions, but may occasionally miss one of the target atoms. No systematic errors seem to result from this possibility.

A very simple model of thermal vibrations is provided as an optional feature of the program. Each target atom is allowed to vibrate spherically symmetrically about its lattice site, entirely independently of its neighbors, with a specified root-mean-square amplitude. The distribution of amplitudes chosen was the triangular approximation to a Gaussian

$$\begin{aligned} P(\rho) &= (2\pi)^{-1/2}\exp(-\tfrac{1}{2}\rho^2) \\ &\approx 1/\sqrt{6}-|\rho|/6, \quad -\sqrt{6}\leq\rho\leq\sqrt{6}, \\ &\approx 0, \qquad\qquad \sqrt{6}\leq|\rho|\leq\infty, \end{aligned} \tag{1}$$

where ρ is the radial displacement from the lattice site in units of the rms amplitude and $P(\rho)d\rho$ is the probability of finding a displacement between ρ and $\rho+d\rho$. Both distributions in Eq. (1) have a zero mean and unit variance. The triangular distribution is very convenient on the machine[13] and has the advantage that no very large amplitude ever occurs.

At each collision, the c.m. scattering angle, Θ, and "time integral," τ, are evaluated from the integrals,

$$\Theta=\pi-2\tan^{-1}\frac{s}{(R_c^2-s^2)^{1/2}}-2s\int_{R_0}^{R_c}\frac{dr}{r^2f(r)}, \tag{2}$$

$$\tau=\int_{R_0}^{R_c}\frac{dr}{f(r)}, \tag{3}$$

where

$$f(r)=[1-s^2/r^2-(1+A)V(r)/AE]^{1/2}, \tag{4}$$

and where s is the impact parameter, E is the initial (laboratory) energy of the primary, A is the mass of the target atom in units of that of the primary, r is the (variable) interatomic separation, $V(r)$ is the interatomic potential, R_0 is the distance of closest approach of the two particles, defined by $f(R_0)=0$, and R_c is the finite range of the potential. The value of τ determines how far the center of mass moves during the interaction and is required in locating the intersection of the laboratory asymptotes of the trajectory of the moving particle The singularities at the lower limits of the integrands of Eqs. (2) and (3) are removed as described before,[7] after which both integrals are amenable to accurate evaluation by Gaussian quadrature.

Since the spatial locations of the target atoms are known *a priori* in this model, the history of a primary is completely determined once its initial and final conditions are specified. The initial primaries are selected by random number techniques[14] from one of two populations:

(1) A distribution of *directions* isotropic about a lattice site in an infinite crystal. Calculations based on this set are referred to hereafter as *isotropic*. It is essential to recognize that these primaries always originate at lattice sites.

(2) A distribution of *positions* uniform over the symmetry element of a particular crystallographic surface of a half infinite crystal. The primaries may escape from the target by passing back through this surface.

Note that integration over all possible sets of the latter kind does *not* lead to the "isotropic" population because of the unique nature of the lattice site as a starting

[13] H. Kahn, U. S. Atomic Energy Commission Report AECU-3259, 1954, pp. 39–41 (unpublished).

[14] The use of random numbers in initialization is merely convenient. Its principal advantage over methods based on regular grids is that it provides a sample of primaries which may be expanded readily. There may also be some slight advantage in reducing bias in the sample, particularly in the isotropic case.

point. The history of a primary is followed, collision by collision, until it is terminated by one of the following conditions.

(1) The primary energy falls below a preset limit, always taken as 25 eV in these calculations.
(2) The particle escapes from the target.
(3) The number of collisions made by the primary exceeds a preset number. This feature is necessitated by the occurrence of channeling.

Most of the calculations to be reported here were based on samples of about 1000 primary atoms. The computer provided distribution functions of various properties of the individual histories in the form of histograms and also evaluated some central measures (e.g., median, mean) of these distributions. The latter analysis has proved to be of limited usefulness because of the nature of the distributions. It was also possible to obtain detailed trajectories of selected primary particles, a feature which proved to be of value in studying channeling.

B. Interatomic Potential

The choice of a suitable interatomic potential for use in the calculation is a difficult one. Although the Bohr (exponentially screened Coulomb) potential was reasonably satisfactory in the random calculations,[7] particularly for Cu atoms slowing down in Cu, it certainly decreases too rapidly with distance to be very useful for atoms separated by as much as half the nearest neighbor distance. On the other hand, a Born-Mayer potential, which gives more reasonable behavior at large separations, is certainly insufficiently strong for close encounters. Accordingly, calculations have been performed for Cu atoms slowing down in Cu, using both potentials,

Bohr,

$$\phi_B(r)=C_B(a_B/r)\exp(-r/a_B), \tag{5}$$

$$C_B=Z_1Z_2e^2/a_B, \tag{6}$$

$$a_B=a_H(Z_1^{2/3}+Z_2^{2/3})^{-1/2}; \tag{7}$$

Born-Mayer,

$$\phi_{BM}(r)=C_{BM}\exp(-r/a_{BM}); \tag{8}$$

where e is the electronic charge, the Z_i are the atomic numbers of the interacting atoms, a_H is the radius of the first Bohr orbit of hydrogen (0.529 Å), and C_{BM} and a_{BM} are constants to be derived from elasticity data (for example). Numerical values of the coefficients for Cu-Cu interactions are given in Table I(a). The Born-Mayer parameters are those of the potential II of Gibson *et al.*,[15] which they employed in their studies of the dynamics of radiation damage in Cu.

The potential actually employed by the computer

TABLE I. Some numerical data used in the calculations.

(a) Interatomic potential parameters for Cu-Cu interactions

Potential	Coefficient, C (keV)	Screening length, a (Å)
Bohr	99.4	0.1218
Born-Mayer (See Ref. 15)	22.5	0.1966

(b) Crystallographic properties of "copper" targets. Nearest neighbor distance 2.5562 Å.

	fcc	bcc	diamond
Coordination number	12	8	4
Lattice constant (Å)	3.6150	2.9516	5.9032
Relative density	1.0000	0.9186	0.4593

(c) Designations of various truncated and eroded potentials

Potential	R_c(Å)	$\phi(R_c)$(eV)
Truncated Bohr	1.2781	0.26
Truncated Born-Mayer		
I	1.2781	33.83
II	1.3556	22.80
III	1.3914	19.01
IV	2.2137	0.29
Eroded Born-Mayer	1.2781	33.83

may be written as

$$\begin{aligned} V(r)&=\phi(r)-\delta\phi(R_c), && 0\le r\le Rc,\\ &=0, && R_c<r<\infty, \end{aligned} \tag{9}$$

where $\phi(r)$ is given by either Eq. (5) or (8) and where δ assumes the values 0 and 1 only.[16] When $\delta=0$, the potential is termed *truncated*; when $\delta=1$, it is referred to as eroded. This procedure was adopted partly to ensure that only two-body collisions occurred, but was also thought to be required by the fact that τ, Eq. (3), is undefined for infinite R_c. Actually, for potentials falling off more rapidly than $1/r$, the equally useful integral

$$\tau^*=\int_s^{R_c} dr\left(1-\frac{s^2}{r^2}\right)^{-1/2}-\tau \tag{10}$$

remains finite as R_c increases without bound, and potential truncation could have been avoided.

The treatment of the potential results in two peculiarities of the model which must be borne in mind. First, there generally will be force-free regions within the crystal. These regions may or may not interconnect, depending on the point symmetry of the crystal and the magnitude of R_c, but, if they are connected, primaries may be "lost" to the void channels. In fact, primaries are lost only if they are initially incident into such void channels, the presence of which is apparently of minor importance in the model. Second, because of the sensitivity of the model to details, the eroded and truncated potentials often give rather different results. In the former case, as the impact parameter approaches R_c, the c.m. scattering angle approaches zero smoothly. The stopping power of this potential is less than if it had not been cut off. With the truncated potentials, however, as the

[15] J. B. Gibson, A. N. Goland, M. Milgram, and G. H. Vineyard, Phys. Rev. **120**, 1229 (1960).

[16] The variable δ may be regarded (as it is by the machine program) as a Boolean variable which tells whether (1, "true") or not (0, "false") to subtract the value $\phi(R_c)$.

impact parameter becomes large, the distance of closest approach will reach R_c before s does and a hard-core scattering will take place off the edge of the potential. For impact parameters in the range

$$[1-(1+A)\phi(R_c)/AE]^{1/2}<s/R_c<1 \qquad (11)$$

the scattering angle (and hence the stopping power) is greater than would be the case for the continuous potential. For primary energies less than $(1+A)\phi(R_c)/A$, hard-core scattering will take place for any impact parameter. The hard-core scattering region introduces into the calculation an artifact which will be discussed in Sec. IIID. A detailed analysis of scattering from truncated potentials has been given recently by Lehmann and Leibfried.[17]

C. Description of the Targets

Early in the calculational program, it became apparent that crystallographic considerations were of major importance. In order to study the effects of lattice symmetry independently of changes in the interatomic potential, two hypothetical structures were employed as targets, in addition to ordinary fcc Cu. Keeping the nearest-neighbor distance the same as in fcc Cu, it is a simple matter to deduce the lattice constants given in Table I(b) for bcc and diamond-structure "Cu." As a matter of convenience, we refer to the latter as dia "Cu." Calculations to study the effects of mass ratio were done, using as primaries the hypothetical "copper" atoms of masses 190.62 ($A=\frac{1}{3}$) and 21.18 ($A=3$). The effects of temperature were studied using two different rms-vibration amplitudes, 0.05 and 0.20 Å, which approximate the behavior of Cu at 0°K and at the melting point, respectively.[18] Several different truncation distances were used in calculations with the Born-Mayer potential: These are shown in Table I(c). Potential I is truncated at half the nearest-neighbor distance of the target structures. Potential II is truncated at 53% of the nearest-neighbor distance so that no connected voids occur in the fcc structure. Potentials III and IV are truncated at distances which prevent interconnecting voids in the bcc and dia structures respectively.

In discussing the results of our calculations, it is convenient to refer to the *transparency*[9] of a crystallographic direction: It is evident from visual examination that crystal models are more transparent when viewed in certain directions than they are when viewed in others. The concept of transparency may be made quantitative by defining ρ_{hkl}, the number of $[hkl]$ row lines passing through a unit area of an (hkl) plane. This definition is, of course, suitable only for cubic crystals, but may be extended easily to other systems. The row density, ρ_{hkl}, is related to the hit probability used by Southern, Willis, and Robinson in their transparency model of sputtering,[9] except that shadowing effects are ignored here. In Table II are listed the values of ρ_{hkl} for some of the most open directions for each of the structures to be considered below: the lower the value of ρ_{hkl}, the more transparent is the direction.

TABLE II. The most open directions of fcc, bcc, and dia "Cu."

$\langle hkl\rangle$ fcc	bcc	dia	Row density ρ_{hkl}(Å^{-2})
...	...	011	0.162
...	111	111	0.199
011	...	...	0.217
...	001	001	0.230
...	...	112	0.282
001	...	...	0.306
...	011	...	0.324
...	...	013	0.363
112	...	...	0.375
...	113	113	0.380
...	...	123	0.429
013	...	...	0.484
...	...	114	0.487
...	133	133	0.500
...	012	012	0.513
111	...	...	0.530
...	...	233	0.538
...	112	...	0.562
123	...	...	0.572

Comparisons between the calculations for the different structures will be facilitated by remembering the close similarity between the bcc and dia structures. In particular, we note that the interatomic spacing along dia $\langle 001\rangle$ is just twice that along bcc $\langle 001\rangle$, and that the spacings along dia $\langle 111\rangle$ are alternately the same as and three times as great as that along bcc $\langle 111\rangle$. The row densities for these directions are the same in the two structures. On the other hand, the interatomic spacing along dia $\langle 011\rangle$ is the same as that along bcc $\langle 011\rangle$, but the row density in dia is half that in bcc. These remarks will be of use in discussing some of the results of our calculations.

III. RESULTS OF THE CALCULATIONS

A. Comparison with Random Model

A series of calculations was performed for Cu atoms slowing down to 25 eV in fcc Cu, using a Bohr potential truncated at half the nearest-neighbor distance. Since

TABLE III. Comparison of lattice and random (Ref. 7) models. Initially isotropic Cu atoms slowing down to 25 eV in fcc Cu. Truncated Bohr potential; static lattice.

Initial primary energy (keV)		1	5	10
$\langle l\rangle$(Å)	Lattice	2.14	2.20	2.24
	Random	2.08	2.18	2.21
$\langle x\rangle$(Å)	Lattice	31.7	59.1	79.7
	Random	27.9	58.8	79.9
$\langle x^2\rangle^{1/2}/\langle x\rangle$	Lattice	1.44	1.35	1.31
	Random	1.20	1.20	1.19

[17] C. Lehmann and G. Leibfried, Z. Physik **172**, 465 (1963).
[18] G. Leibfried, in *Handbuch der Physik*, edited by S. Flügge (Springer-Verlag, Berlin, 1955), Vol. 7, Part 1, p. 264.

TABLE IV. Average directions of trajectories involving >250 collisions. 1- to 10-keV Cu slowing down in fcc Cu. Truncated Bohr potential. Static lattice.

Initial primary directions	Isotropic	⟨011⟩	⟨001⟩	⟨111⟩
Total number of primaries	5056	5836	6968	6207
Fraction >250 collisions	0.011	0.789	0.601	0.226
Number of long trajectories analyzed for direction	56	2145	1875	1227
Fraction of long trajectories with average direction near				
⟨011⟩	0.77	0.997	0.005	0.035
⟨001⟩	0.05	0.000	0.990	0.003
⟨112⟩	0.05	0.002	0.002	0.014
⟨013⟩	0.02	0.000	0.001	0.003
⟨111⟩	0.02	0.000	0.000	0.937
⟨123⟩	0.04	0.000	0.000	0.001
Other	0.05	0.001	0.002	0.007

$\phi_B(R_c)$ is only 0.26 eV, the effect of truncating the potential is very small and the results for initially isotropic primaries may be compared directly to the earlier random model calculations.[7] A comparison is made in Table III of $\langle l\rangle$, the mean distance between collisions; $\langle x\rangle$, the mean penetration[19]; and the ratio $\langle x^2\rangle^{1/2}/\langle x\rangle$, which is a measure of the skewness of the distribution of penetrations. The close correspondence of the values of $\langle l\rangle$ supports the value chosen in the earlier work for the "free-flight" distance. The small differences may probably be attributed to the effects of the approximation used in treating the time integral in the random calculation. The values of $\langle x\rangle$ are not actually in as good agreement as appears in Table III, since the lattice model values were computed omitting those primaries (about 1% of the total) which made exceedingly long flights. These trajectories were so long[20] that $\langle x\rangle$ is probably undefined in the lattice model, at least with the Bohr potential. Finally, the ratio $\langle x^2\rangle^{1/2}/\langle x\rangle$ shows the penetration distribution to be significantly more skewed in the lattice model than in the random, an effect which is minimized in the table because of the omission of the longest flights from the distribution. Since one of the discrepancies from experiment noted in the random calculations was the insufficient skewness of the range distributions,[7] it appears that inclusion of the lattice in the model affords a real improvement, even for initally isotropic primaries.

B. Analysis of the Long Trajectories

In Table IV are lumped together some results of calculations for 1.0-, 2.5-, 5.0-, 7.5-, and 10.0-keV primaries slowing down to 25 eV in fcc Cu according to the truncated Bohr potential. The fraction of trajectories which involved more than 250 collisions is to be compared with an estimate of $\sim 10^{-5}$ deduced from the older random calculations for 10-keV Cu primaries. Directional analyses showed that most of the long trajectories were oriented parallel to the most open directions of the fcc structure. The results in Table IV suggest that the long trajectories represent primaries which are

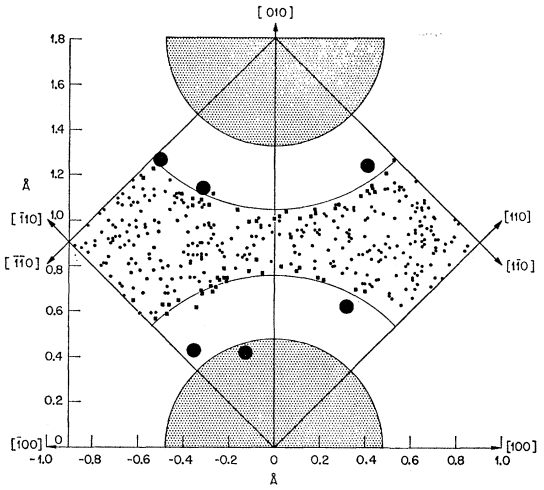

FIG. 1. The points at which [001] channeled 1-keV Cu primaries entered an fcc Cu crystal are shown by the dots. The larger filled circles show the entry points of primaries channeled in other directions. The large shaded circles show the locations of the target atoms, their radii representing the distance of closest approach in a head-on collision at 1 keV. The circles of larger radius represent the impact parameter for transfer of 10 eV at 1 keV. Truncated Bohr potential, static lattice.

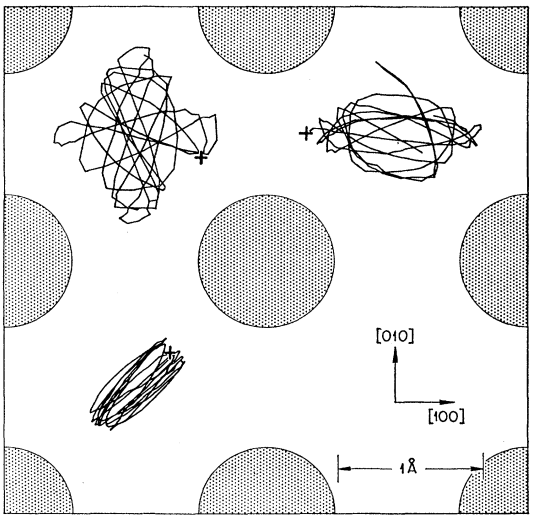

FIG. 2. Projection of some [001] channel trajectories onto the (001) surface of fcc Cu. 1-keV Cu slowing down according to the truncated Bohr potential. The points at which the primaries entered the crystal are shown by the crosses. Each primary penetrated approximately 300 Å into the crystal in the part of its trajectory shown (250 collisions).

[19] We use the terms *penetration* and *spread* for the components of the range parallel to and perpendicular to the original direction of motion of the primary, respectively. See Ref. 7 for definitions of other range quantities.

[20] In one of the early studies of the lattice model with the Bohr potential, one primary was followed for a distance of some 6×10^4 Å, at which point the run was terminated by intervention of the machine operator. This behavior was responsible for including the option of terminating an individual trajectory after a preset number of collisions.

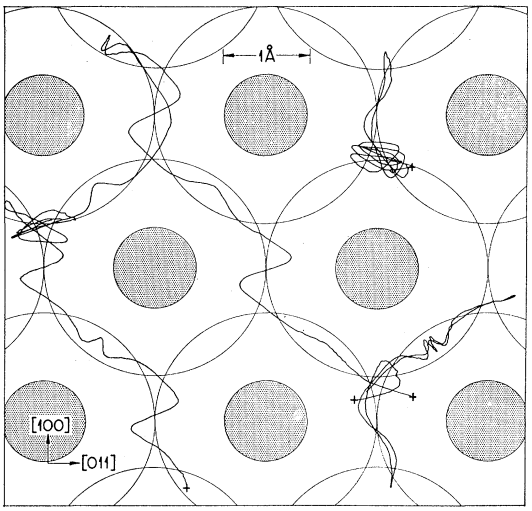

FIG. 3. Projection of some [01$\bar{1}$] channel trajectories onto the (01$\bar{1}$) surface of fcc Cu. 1-keV Cu slowing down according to the truncated Bohr potential. The points at which the primaries entered the crystal are shown by the crosses. Each primary penetrated approximately 300 Å into the crystal in the part of its trajectory shown (250 collisions).

channeled, that is, which are constrained by large numbers of very glancing collisions to move in regions of low potential surrounded by relatively closely packed atomic rows. That this is indeed the correct explanation may be seen from Fig. 1, which shows the points at which the eventually channeled atoms entered the crystal in a calculation for 1-keV Cu atoms normally incident on the (001) surface. Those particles which made glancing collisions at the surface continued to do so and moved solely in the [001] direction. A few other primaries suffered more drastic encounters on entering the crystal, but were eventually channeled in other directions, principally ⟨011⟩. Similar results have been obtained for particles incident upon the (011) surface also.

C. Individual Channeled Atoms

So many primaries were channeled when calculations were made with the Bohr potential that the computer time required to obtain statistical information on the distribution of penetrations was prohibitively great. Attention was concentrated, therefore, on the behavior of individual trajectories, some of which are shown in Figs. 2–4. These individual trajectories show very clearly the nature of channeling, namely, the constraint exerted by the lattice through large numbers of correlated glancing collisions. Figures 2 and 3 show the trajectories of 1-keV Cu atoms, initially incident in the [001] and [01$\bar{1}$] directions, respectively, slowing down in fcc Cu according to the truncated Bohr potential. The [001] channel events are stable, that is, restricted to a single channel, and have shapes related to the symmetry elements of the crystal. Thus, the event in the lower left quadrant of Fig. 2 took place almost solely in the ($\bar{1}$10) plane in which it started, this being a mirror plane of the crystal. The event in the upper right quadrant was somewhat restricted to the (010) plane in which it began, but since this plane, being unoccupied by atoms, is a symmetry element only of the projection, the restriction of the event was less complete. The [01$\bar{1}$] channel trajectories shown in Fig. 3 are less stable than are the [001] events, only the upper right hand trajectory being restricted to a pair of neighboring channels. (Note that ⟨011⟩ channels occur in pairs, the axes lying in the triangular regions where three atomic potentials come together.) In addition to a component of motion around the channel axis, these trajectories have another component which tends to take them around the outside of a close-packed atomic row. Because of this component, the trajectories drift fairly easily from one channel to another. Although no example is shown in the figure, it is clearly possible for a sort of "macrochannel" to be imagined in which the trajectory surrounds a close-packed row and is constrained by a hexagonal array of other rows. Figure 4 displays the trajectories of some [001] channeled particles in bcc "Cu" slowing down according to truncated Born-Mayer potential III. It is apparent that these trajectories are not stable and that "macrochanneling" may occur.

D. "Trapped" Channel Trajectories

When calculations were performed for Cu atoms slowing down according to truncated Born-Mayer potential I, some of the trajectories involving the largest numbers of collisions were not also of great length. The frequencies of such trajectories are listed in Table V for each of the three structure types. In every case, when "trapping" occurred, the direction of the trajectory was very nearly perpendicular to the direction of the nearest-neighbor "bonds" of the crystal (⟨011⟩ in fcc, ⟨111⟩ in bcc and dia). In the fcc and bcc structures,

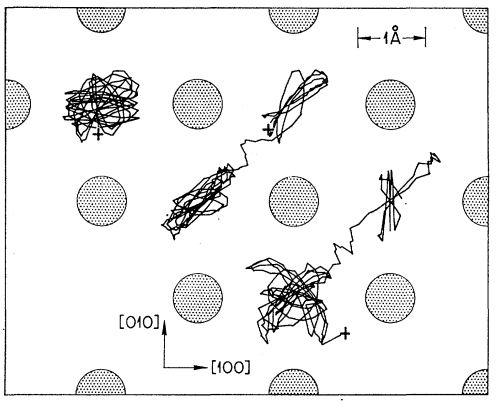

FIG. 4. Projection of some [001] channel trajectories onto the (001) face of bcc "Cu." 5-keV Cu slowing down according to truncated Born-Mayer potential III. The points at which the primaries entered the crystal are shown by the crosses. Each primary penetrated approximately 300 Å into the crystal in the part of its trajectory shown (175 collisions for upper left event; 250 collisions for the other two).

TABLE V. Frequency of "trapped" trajectories involving >250 collisions. 1- to 10-keV Cu slowing down in "Cu" according to truncated Born-Mayer potential I.

Structure	Initial primary direction	Total number of primaries	Frequency of "trapped" trajectories (%)
fcc	Isotropic	6035	0.58
	⟨111⟩	6036	0.60
	⟨013⟩	6033	0.55
	⟨112⟩	6164	0.29
	⟨001⟩	6033	0.96
	⟨011⟩	7492	0.49
bcc	Isotropic	5035	0.70
	⟨011⟩	5226	1.44
	⟨001⟩	6145	0.21
	⟨111⟩	6702	0.54
dia	Isotropic	5012	0.22
	⟨001⟩	5438	0.18
	⟨111⟩	5198	0.27
	⟨011⟩	6349	0.19

the most prominent individual directions correspond to those of the channels whose axes are the perpendicular bisectors of a sequence of "bonds" (⟨001⟩ in fcc and ⟨011⟩ in bcc). These are also the initial primary directions showing the highest frequencies of "trapping." When the potential was eroded at half the nearest-neighbor distance or when the truncation distance was increased to remove connections between void regions (potentials II in fcc, III in bcc, IV in dia), there were no "trapped" trajectories observed. Examination of some individual trajectories showed the "trapping" to occur when the energy of a primary had been sufficiently reduced (to ~100 eV) that it made principally hard-core collisions and then found itself moving in the same plane as a nearest neighbor "bond." In these circumstances, it sometimes was compelled to make a long series of hard-core collisions alternately with a pair of

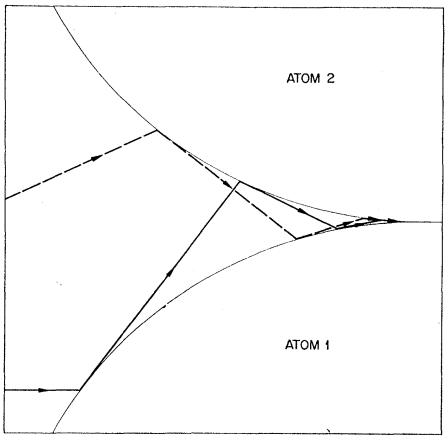

FIG. 5. Schematic representation of the "trapping" of a primary by hard core collisions with a pair of nearest neighbors. The sketch assumes $A=1$.

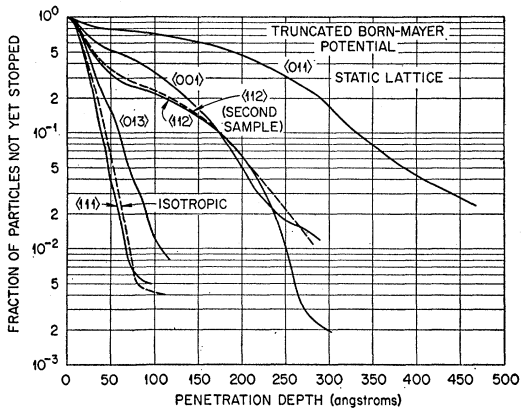

FIG. 6. Integral penetration distributions calculated for 5-keV Cu slowing down to 25 eV in fcc Cu ($A=1$). Truncated Born-Mayer potential I. Static lattice. Initial primary directions as shown on curves.

neighboring atoms, each collision involving only a very small transfer of energy, as illustrated in Fig. 5. If the primary had a component of motion perpendicular to the plane of the figure, one would expect the trapping to be unstable and the particle to proceed after only a few collisions. Hence, the events listed in Table I presumably represent only the extreme cases, and other trajectories are probably affected by "trapping" also. The incidence

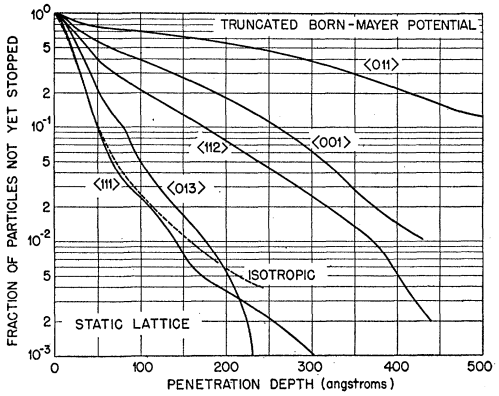

FIG. 7. Integral penetration distributions calculated for 5-keV "light Cu" slowing down to 25 eV in fcc Cu ($A=3$). Other conditions as in Fig. 6.

of "trapping" is lower in the diamond structure than in fcc or bcc because here the nearest-neighbor "bonds," although perpendicular to the ⟨011⟩ channels, are not bisected by the channel axes, but instead border the channel. Hence, the crystal is less effective in producing the "trapped" trajectories than are the fcc and bcc lattices. While "trapping" is a consequence of using truncated potential I, that is, of the hard-core scattering region, it also illustrates the effectiveness of channeling in focusing primaries into certain preferred directions of the lattice and demonstrates the extreme sensitivity of the lattice model calculations to apparently minor details.

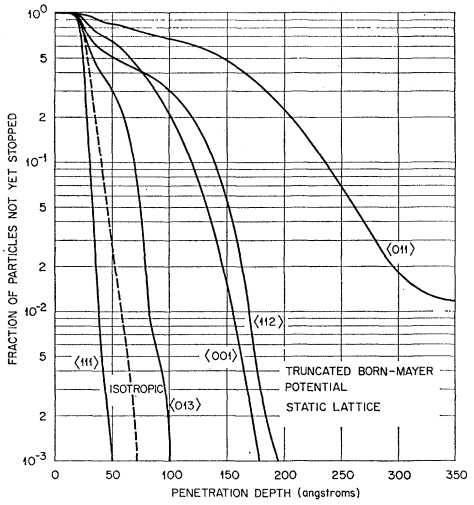

FIG. 8. Integral penetration distributions calculated for 5-keV "heavy Cu" slowing down to 25 eV in fcc Cu ($A=\frac{1}{3}$). Other conditions as in Fig. 6.

E. Penetration Distributions for fcc Crystals

In Figs. 6 through 10 are displayed the integral penetration distributions calculated for various 5-keV "Cu" atoms slowing down to 25 eV in fcc Cu according to truncated Born-Mayer potential I. The initial directions of the primaries are the five most open directions of the fcc lattice, as well as the isotropic set. Each curve is based on an ensemble of approximately 1000 primary particles.[21] As can be seen from the two independent ⟨112⟩ curves shown in Fig. 6, the reproducibility of the computations is good except in the lowest decade. Here only 1 to 10 particles generally remain in the ensemble and statistical fluctuations are large. Numerous comparisons of independent samples suggest that the precision of any point on the curves is derivable according to Poisson statistics from the number of particles contributing to it.

The various initial primary directions yield distributions falling roughly into three groups. The ⟨011⟩ penetrations are the greatest, whatever the mass of the primary or the vibrational amplitude of the target particles. The ⟨001⟩ and ⟨112⟩ penetrations are intermediate and the ⟨013⟩ and ⟨111⟩ penetrations are least, differing very little from the isotropic. (It is well to point out again that the isotropic curves plotted refer to primaries, all of which originate at lattice sites. An appropriate average over the various ⟨*hkl*⟩ curves will *not* yield the same isotropic result.) The general disposition of these distributions (except for the crossing of the ⟨001⟩ and ⟨112⟩ curves) is as expected from transparency considerations. It may be seen by comparison of Figs. 6, 7, and 8 that dispersion of the distributions is greatest for the light primaries and least for the heavy ones. Further,

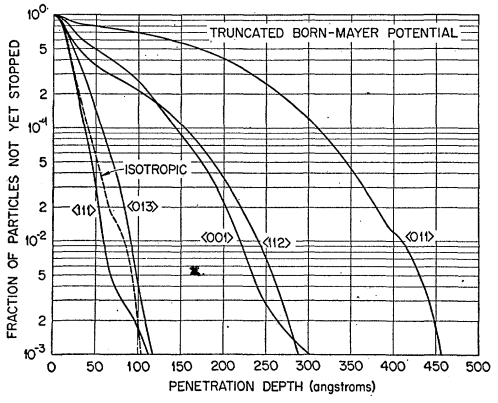

FIG. 9. Integral penetration distributions calculated for 5-keV Cu slowing down to 25 eV in fcc Cu. Rms lattice vibrational amplitude 0.05 Å (~0°K). Other conditions as in Fig. 6.

[21] The procedure was to run the computer either until 1000 primaries had slowed down from the initial energy to less than 25 eV or until one hour of machine time had elapsed. The total number of primaries was often >1000 because of (1) particles escaping from the target, (2) particles making >250 collisions, and (3) particles directly incident into void channels, none of which were counted in accumulating the desired 1000 events. Only the escaping particles are omitted in the distribution functions, however.

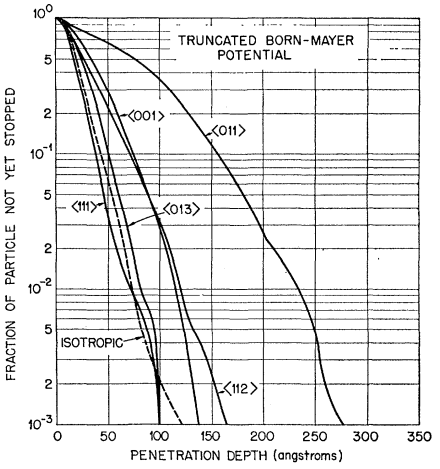

FIG. 10. Integral penetration distributions calculated for 5-keV Cu slowing down to 25 eV in fcc Cu. Rms lattice vibrational amplitude 0.20 Å (~1350°K). Other conditions as in Fig. 6.

TABLE VI. Effects of mass ratio and of thermal vibration amplitude on the penetration of 5-keV "Cu" into fcc Cu. Truncated Born-Mayer potential I.

Initial primary direction	Median penetrations (Å) Mass ratio effect (static lattice) $A=3$	$A=1$	$A=\frac{1}{3}$	Thermal effect ($A=1$) rms=0.05 Å	rms=0.20 Å
⟨011⟩	235	191	145	174	77
⟨001⟩	69	59	65	49	34
⟨112⟩	38	29	52	31	27
⟨013⟩	28	24	34	24	24
⟨111⟩	20	19	24	18	17
Isotropic	19	19	28	19	20

comparison of Figs. 6, 9, and 10 shows that increasing the "temperature" reduces the dispersion of penetrations. Table VI lists the *median* penetrations for these five sets of conditions. Since all particles contribute to the median, the precision of the numbers is about ±3%.

The crossing of the ⟨001⟩ and ⟨112⟩ distributions, observable in all but Fig. 7, is connected with the truncation of the potential at half the nearest neighbor distance. When the truncation was done at 53% of the nearest-neighbor distance, thus eliminating the connections between the void regions, or when the potential was eroded, these curves did not cross, but the ⟨112⟩ distribution always lay below the ⟨001⟩, in a manner similar to Fig. 7. This behavior raises the important question of the influence on the results of the precise treatment of the potential. Figure 11 shows the curves computed for ⟨001⟩ incident 5-keV Cu primaries slowing down in fcc Cu for each of three treatments of the Born-Mayer potential. The distributions differ rather

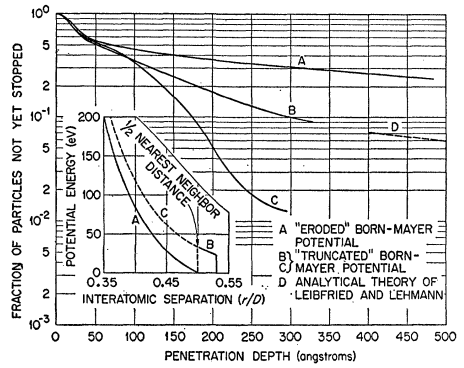

FIG. 11. The effect of variations in the potential on the penetration of 5-keV Cu into fcc Cu. Primaries initially incident in ⟨001⟩. Static lattice. The insert shows the outermost portion of each potential function. Curves B and C represent truncated Born-Mayer potentials II and I, respectively.

dramatically in the region of the greatest penetrations, but the least penetrating half or two-thirds of the primaries are not too seriously affected. Table VII displays the median penetrations computed for 5-keV primaries for a number of different initial directions and for each Born-Mayer potential. The medians do not vary significantly except for the two most open directions and the effect is large only for ⟨011⟩. The more penetrating primaries, however, are more seriously affected than the table indicates, Fig. 11 being typical. The remarks made in Sec. IIB about the hard core scattering region are sufficient to explain the curves of Fig. 11. This figure also shows the analytical channeling theory of Lehmann and Leibfried,[22] here extrapolated well beyond its region of validity for purposes of comparison.

In order to emphasize the nature of the distribution functions shown in Figs. 6 to 10, the *differential* distributions of two of them are shown as histograms[23] in Fig. 12. The isotropic histogram shows a unimodal shape, peaking near 15 Å, and slightly skewed to the right. The ⟨001⟩ histogram, on the other hand, is bimodal, the first peak coinciding with the isotropic one, the second occurring near 100 Å. It seems quite natural to interpret this bimodal distribution on a two-group basis, the first mode associated with an isotropic type of slowing down of the incident primary, while the second is associated with the channeled particles.

TABLE VII. Effects of potential treatment on the penetration of 5-keV Cu into fcc Cu. Born-Mayer potential.

Initial primary direction	Median penetration (Å) Eroded	Truncated I	Truncated II
⟨011⟩	>700	191	233
⟨001⟩	71	59	54
⟨112⟩	32	29	28
⟨013⟩	28	24	24
⟨111⟩	21	19	19
Isotropic	20	19	19

F. Influence of Crystal Structure on the Penetration

In Fig. 13 are shown the integral penetration distributions calculated for 5-keV Cu atoms slowing down in bcc and dia "Cu" according to truncated Born-Mayer potential I. The initially isotropic primaries penetrate more deeply into the dia structure than they do into the

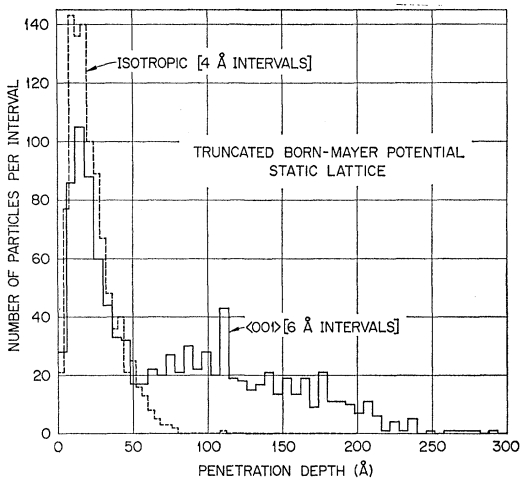

FIG. 12. Differential penetration distributions for initially isotropic and initially ⟨001⟩ 5-keV Cu primaries slowing down to 25 eV in fcc Cu. Other conditions as in Fig. 6.

[22] C. Lehmann and G. Leibfried, J. Appl. Phys. **34**, 2821 (1963).

[23] Histograms of the type shown in Fig. 12 were computed by the machine. For compact presentation of computations, however, the integral form of Figs. 6 to 10 has been preferred. The latter have the additional advantage of being in the form used by Davies *et al.* (Refs. 3, 11, 12) for presentation of their experimental data.

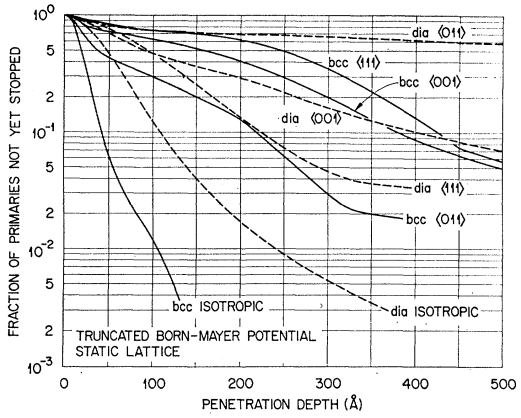

FIG. 13. Integral penetration distributions calculated for 5-keV Cu atoms slowing down to 25 eV in bcc and dia "Cu." Truncated Born-Mayer potential I. Static lattice. Initial primary directions as shown on curves.

bcc, as is expected from the greater density of the latter. In fact, the increase in penetration on going from the fcc or bcc structure to the dia is somewhat greater than expected from the density changes alone. Figure 14 shows the median penetration of initially isotropic primaries into each of the three structures as a function of the initial primary energy. Within the uncertainties of the calculated values ($\sim\pm 3\%$), the fcc and bcc penetrations differ as expected from the densities. As the figure shows, however, the dia penetration is $\sim 20\%$ larger than expected. This seems to be a specific structural effect.

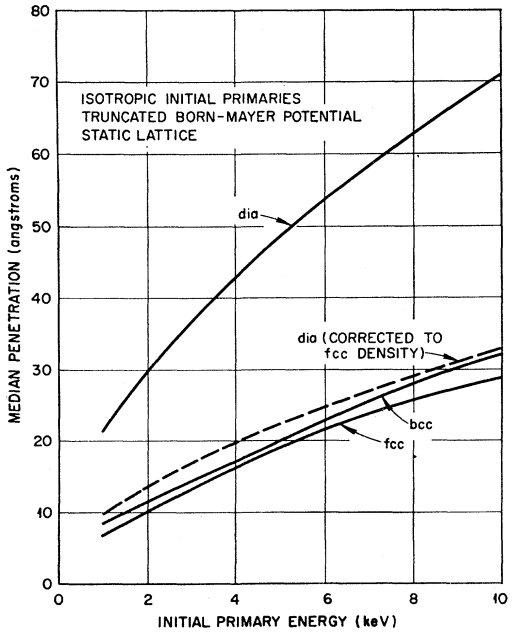

FIG. 14. Median penetrations of initially isotropic Cu primaries slowing down to 25 eV in "Cu" as functions of the type of crystal and the initial primary energy. Other conditions as in Figs. 6 and 13.

The dramatic effect of channeling in increasing the penetration of primaries in open crystallographic directions of the bcc and dia structures is evident in Fig. 13. The general disposition of the bcc curves, like that of the fcc penetration distributions, is as expected from transparency considerations, but the situation in dia is more complicated as can be seen from the crossing of the ⟨111⟩ and ⟨001⟩ curves at a moderate penetration. Figure 15 displays the median penetrations calculated for the principal directions of each of the three structures as functions of the initial primary energy, while Fig. 16 shows the calculated median spreads[19] of the bcc and dia distributions (the fcc curves are very similar to the bcc and are omitted for clarity). It will be noted that for each structure there is a complementary relation between penetration and spread.

With the exception of dia ⟨001⟩ and ⟨111⟩, the median penetrations of Cu atoms into the three targets (Table V, Fig. 15) fall in the order expected from the row densities of Table II. That is, the penetration is greatest in the most open direction (dia ⟨011⟩) and least in the least open (fcc ⟨111⟩) of the directions studied. The exceptional cases can be understood in terms of the interatomic spacings in the incident directions. As Table II indicates, the transparencies of the dia and bcc ⟨001⟩ and ⟨111⟩ directions are the same, leading one to expect similar penetrations. However, the greater interatomic spacings in the dia rows, particularly the long ⟨111⟩ spacing, should permit many particles to "leak out of" these channels which would not do so in bcc. This increased "leakage" will lead to a decrease in the penetration and a concomitant increase in the spread, as observed in the calculations. Since the "leakage" from dia ⟨111⟩ channels should be greater than from ⟨001⟩, the crossing of the respective penetration distributions in Fig. 13 can be understood. The change of this crossing point with energy produces the crossing of the median penetration curves of Fig. 15. At the lowest energies,

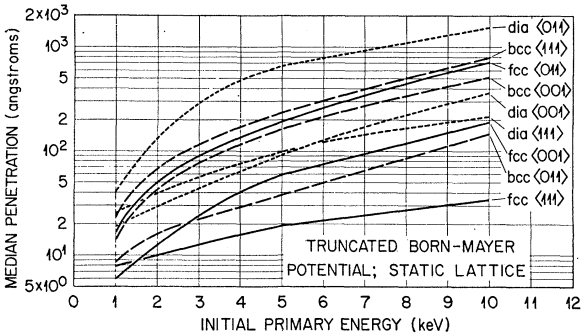

FIG. 15. Median penetrations of Cu primaries slowing down to 25 eV in "Cu" as functions of the initial direction, the type of crystal, and the initial primary energy. Other conditions as in Figs. 6 and 13.

the penetrations no longer occur in the transparency order, but they are then so small (~10 Å) that channel motion has no real opportunity to develop. Finally, it must be pointed out that the truncation of the potential may play some part in the complexity of the dia penetration distributions and in their relation to the bcc curves, but insufficient calculations have been performed to assess this point.

G. Miscellaneous Results

The machine reported some information on the primaries which escaped from the targets. For $A=1$, the number of these was too small (~0.2% of the ensemble) in the fcc and bcc cases to be usefully analyzed. No heavy ($A=\frac{1}{3}$) primaries escaped from fcc Cu. The results for light ($A=3$) primaries in fcc are shown in Table VIII, which also displays the escape probabilities for some ⟨001⟩ incident primaries ($A=1$) in the dia structure. The latter results show a slight tendency for a decrease in the escape probability with increasing energy, as well as a tendency for more particles to escape from the more open dia structure than from fcc and bcc. It should be emphasized that the escape probabilities include only those particles having energies above 25 eV; hence, experimental "reflection" coefficients might be substantially larger.

The final energies of the primaries should reflect the properties of the scattering law. For example, for a hard-core scattering law and $A=1$, the final energies should be distributed uniformly between 0 and 25 eV. A careful study of the machine histograms for Cu primaries slowing down in fcc Cu according to truncated Born-Mayer potential I showed the distribution of final energies to be uniform below 25 eV, all deviations being consistent with the expectations of Poisson statistics. With this potential, *only* hard-core scattering takes place below about 67 eV (for $A=1$), which accounts for the result. A similar analysis for potential II showed the distribution of final energies to be slightly peaked near 25 eV, a consequence of the increased importance of forward scattering when the hard-core region in the potential is made less important. In both of these analyses, the extreme channeled particles were omitted. They would, of course, contribute a further excess of particles, just below 25 eV.

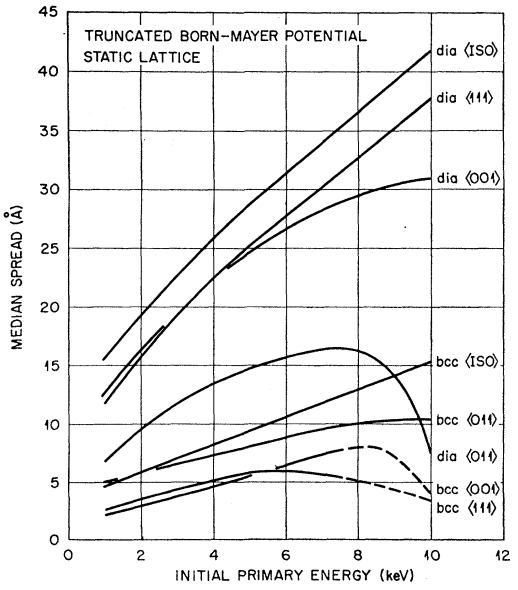

FIG. 16. Median spread of Cu primaries slowing down to 25 eV in "Cu" as functions of the initial direction, the type of crystal, and the initial primary energy. Other conditions as in Figs. 6 and 13.

TABLE VIII. Probability of primaries escaping from targets.

(a) 5-keV light "Cu" in fcc Cu ($A=3$); truncated Born-Mayer potential I; static lattice.

Initial primary direction	Percent primaries escaping
⟨111⟩	11.3
⟨013⟩	8.7
⟨112⟩	8.2
⟨001⟩	5.4
⟨011⟩	3.4

(b) ⟨001⟩ incident Cu in dia "Cu" ($A=1$); truncated Born-Mayer potential I; static lattice.

Initial primary energy (keV)	Percent primaries escaping
1.0	1.8
2.5	2.0
5.0	1.1
7.5	0.5
10.0	0.6

Tables IX and X display the distributions of secondary particle energies produced by 5-keV Cu atoms slowing down in fcc and dia "Cu." In the former case, primaries initially moving in the most open directions produce many more low-energy secondaries than do those selected from the isotropic population. In the most open direction, this is accompanied by a decrease in the number of high-energy secondaries. The diamond structure secondaries are divided into two groups: "A" secondaries originate from one of the two interpenetrating fcc sublattices of which this crystal is con-

TABLE IX. Production of secondaries by 5-keV Cu atoms in fcc Cu. Truncated Born-Mayer potential I. Static lattice.

Initial primary direction	Secondaries produced per primary with energies (eV)[a] >25	>50	>100	>250
⟨011⟩	40.7	22.2	10.0	2.8
⟨001⟩	25.7	17.2	10.3	4.5
⟨112⟩	18.6	12.6	7.9	4.1
⟨013⟩	14.2	11.1	7.8	4.7
⟨111⟩	11.6	8.9	6.3	3.9
Isotropic	12.1	9.4	6.6	4.1

[a] Precision of tabular values is about ±0.1.

TABLE X. Production of secondaries by 5-keV Cu atoms in dia "Cu." Truncated Born-Mayer potential I. Static lattice.

Initial primary direction	Secondaries produced per primary with energies (eV)[a] >25 A	>25 B	>50 A	>50 B	>100 A	>100 B	>250 A	>250 B
⟨011⟩	8.6	8.7	5.4	5.4	3.0	3.0	1.4	1.4
⟨111⟩	7.0	9.1	4.7	6.7	2.9	4.6	1.5	2.7
⟨001⟩	8.8	8.8	6.0	6.1	3.8	3.9	2.1	2.1
Isotropic[b]	6.5	6.8	4.9	5.2	3.3	3.7	2.0	2.3

[a] Precision of tabular values is about ±0.1.
[b] Primaries originated from *A* sites.

structed, "*B*" secondaries from the other. There is a slight excess of high-energy "*B*" secondaries in the isotropic case. These secondaries are (presumably) nearest neighbors of the "*A*" sites from which the primaries originate. The similar excess of "*B*" secondaries occurring for ⟨111⟩ incident primaries results from the particular view of the crystal chosen for the calculations. The surface of the target was (111), that is, contained only "*A*" atoms, and the primaries were incident along $[\bar{1}\bar{1}\bar{1}]$, that is, the long ⟨111⟩ interatomic spacing occurred first behind each surface atom. Thus, to the incident primary, there appeared to be an excess of *B* atoms near the surface of the crystal. As in the fcc calculations, the number of low-energy secondaries is increased for primaries incident in the more open directions, although the effect is less than it is for fcc, and, again, there is a decrease in the number of high-energy secondaries for the most open direction.

IV. COMPARISON WITH EXPERIMENT

A detailed quantitative comparison of our calculations with experiments is not yet possible. The great sensitivity of the results to the detailed treatment of the potential precludes such a comparison, although at the same time it supports the suggestion[22] that a careful experimental study of the most penetrating particles may be used to provide information about the potential for interatomic separations near half the smallest crystal values. Figure 17 shows some of the experimental data recently obtained by Piercy, Davies, McCargo, and Brown[11] on the penetration of 40-keV $^{85}Kr^+$ ions into monocrystalline Al (mass ratio $A=\frac{1}{3}$). The close similarity of this figure to Figs. 6 to 10 is evident, a fact which gives us considerable confidence in our model. On the other hand, the experimental curves show rather less dispersion of the penetrations with direction than do the theoretical ones: The median ⟨011⟩ penetration is only about twice the median ⟨111⟩ penetration in the experiments, whereas it is about six times greater for 5-keV "heavy Cu" in fcc Cu, for which *A* is also $\frac{1}{3}$ (Fig. 8 and Table V). At least part of this difference is certainly attributable to temperature effects (Figs. 9 and 10; Table V). The influence of experimental factors, such as the presence of dislocations in the target crystals and the presence of an oxide film on the target surface,[24] and the possible role of electronic energy losses must be borne in mind. Finally, there is no way of which we are aware to decide what sort of potential is appropriate for Kr-Al interactions. In spite of these difficulties, however, it seems clear that our model gives an essentially correct picture of the slowing down of energetic atoms in crystals.

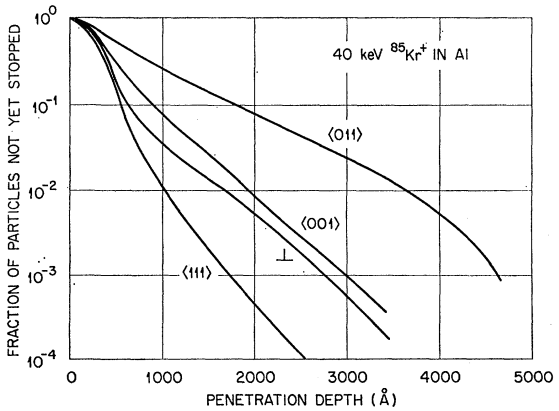

FIG. 17. Experimental data of Piercy, Davies, McCargo, and Brown (Ref. 11) for the penetration of 40-keV $^{85}Kr^+$ into an Al monocrystal. The curve marked ⊥ was obtained at normal incidence (9° from ⟨112⟩); the others were obtained with the beam 28° from the surface normal. The penetrations have been corrected for the angle of incidence.

Lutz and Sizmann[25] have recently reported the occurrence of a deeply penetrating component in studies of the penetration of $^{85}Kr^+$ ions into monocrystalline Cu. They find this component to be particularly strong for ⟨011⟩ incidence. The penetrations which they observe are somewhat smaller than would be expected from the experiments of Davies *et al.*,[3,11,12] but until a full account of their experiments is available, the reliability of their technique cannot be assessed.

The occurrence of a strongly penetrating component in the calculated distribution of penetrations is a consequence of the channeling of the incident atoms in certain directions, of which the most important in the fcc, bcc, and diamond structures are listed in Table II. The experimental data of Piercy, Davies, McCargo, and Brown[11] may be taken as reasonably direct evidence of the physical reality of channeling, at least in the three most open directions of fcc. Nelson and Thompson[26] have observed faint streaks connecting the ⟨011⟩ spots in sputtering ejection patterns from the 25- to 75-keV Ar^+ ion bombardment of monocrystalline Cu, which they attribute to channeling of Cu recoils between {111} planes. Although this is by no means the only possible explanation of their observations, it may be indirect

[24] G. R. Piercy and J. A. Davies, Atomic Energy of Canada Ltd. (private communication).
[25] H. Lutz and R. Sizmann, Phys. Letters **5**, 113 (1963); Z. Naturforsch. (to be published).
[26] R. S. Nelson and M. W. Thompson, Phys. Letters **2**, 124 (1962).

evidence for ⟨112⟩ channeling. Nelson and Thompson have recently reported[27] that the transmission of 75-keV H^+ ions through thin Au crystals is greatly enhanced when the ions are incident along ⟨011⟩ directions. There is some possibility that Tel'kovskii's observation[28] of the penetration of several light ions through a thin Ag film may be associated with channeling. Nelson and Thompson[27] also find the apparent reflection of 50-keV H^+, He^+, Ne^+, and Xe^+ from (011) Cu surfaces to be reduced for certain directions of incidence. All of the fcc channels listed in Table II appear to be observed for H^+ and Ne^+; their curve for Xe^+ shows evidence of ⟨112⟩, ⟨013⟩, and ⟨111⟩ channeling.[29] Unfortunately, these reflection experiments are not unequivocal, since the "reflected" ion current is made up of indistinguishable contributions from reflected bombarding ions, sputtered target ions, and secondary electrons ejected from the collector by energetic reflected or sputtered ions or neutrals. Experiments of this kind can be improved, however, and offer some promise for the study of channeling.

Experimental data on the orientation dependence of the sputtering yield of monocrystalline targets[9,30] may also be regarded as supporting the physical reality of channeling. Put otherwise, the occurrence of channeling can be used to provide a plausible foundation for the so-called "transparency" models of sputtering.[9] These models are based on the idea that bombarding ions may be divided into two groups, one of which makes a collision within one crystal coherence length of the surface, the other of which does not. The crystal is taken as an array of hard spheres whose diameter defines the cross section for colliding near the surface and the sputtering yield is then related in a simple manner to the bombarding particle energy and this cross section. In terms of our calculation, we would describe the two groups of particles as "channeled" and "nonchanneled," the usefulness of such a division being evident from Fig. 12. The cross section defined by the hard spheres is to be interpreted as a cross section for "nonchanneling." It is not at all surprising, therefore, that analysis of experimental data[9] yields a much larger cross section (by about a factor 4) than would be expected from a hard-core approximation to the scattering from the Bohr potential.

[27] R. S. Nelson and M. W. Thompson, Phil. Mag. (to be published).

[28] V. G. Tel'kovskii, in *Proceedings of the Third International Conference on Ionization Phenomena in Gases, Venice, 1957* (Societa Italiana di Fizica, Milan, 1957), pp. 1079–1092.

[29] Our interpretation of Nelson's and Thompson's experiments differs in some respects from theirs (Refs. 26, 27). Additional experiments can be performed which should decide between their views and ours.

[30] O. Almen and G. Bruce, Nucl. Instr. Methods **11**, 257 (1961); V. A. Molchanov, V. G. Tel'kovskii, and V. M. Chicherov, Dokl. Akad. Nauk SSSR **137**, 58 (1961) [translation: Soviet Phys.—Dokl. **6**, 222 (1961)]; V. A. Molchanov and V. G. Tel'kovskii, Izv. Akad. Nauk SSSR, Ser. Fiz. **26**, 1359 (1962); R. L. Cunningham, K. V. Gow, and J. Ng-Yelim, J. Appl. Phys. **34**, 984 (1963); G. D. Magnuson and C. E. Carlston (to be published).

V. DISCUSSION

The trajectories of channeled primaries are of a wide variety of types. At one extreme are those in which the particle moves almost along a channel axis, experiencing only very minor deflections at each collision. Lehmann and Leibfried[22] have developed an analytical treatment of these extreme events, which is valid for perhaps the most penetrating one percent of the incident primaries in the more open fcc directions. As Fig. 11 shows, their theory is quite compatible with our machine calculations using truncated Born-Mayer potential II, which is most nearly similar to their model.

The effects of channeling on penetration distributions are so dramatic that it is natural to seek other consequences of this mode of motion of energetic atoms in crystals. It is characteristic of channeled primaries that they transfer relatively small increments of energy in their collisions with lattice atoms, as Tables IX and X show. We have recently used a much simplified model of channeling as the basis for a modified theory of the radiation damage displacement cascade,[31] obtaining a result in which the number of displacements is a nonlinear function of the initial primary energy. In their machine studies of radiation damage in hexagonal BeO and some fcc and bcc crystals, Beeler and Besco[32] have found significant decreases (by factors of 2 to 10) in the number of displacements produced by channeled primaries as compared to the number produced by nonchanneled ones. Since channeling provides a mechanism for the long-range transport of energy and mass, it must be considered as an alternative to Silsbee focusing[15,33] in producing many of the effects in radiation damage which have been attributed to this process. Swanson, *et al.*,[34] attribute the enhancement of neutron irradiation damage which they observed in cold-worked Al to the disruption of channeling by dislocations. Among the differences between the two mechanisms, which may be of value in separating their effects experimentally, the following may be cited:

(1) Channeling is a high-energy effect, whereas focusing is principally operative at low energies.

(2) Channeling is operative in relatively open crystal structures, such as dia, where focusing is difficult or impossible.

(3) Channel trajectories starting directly from a lattice site are impossible in the more closely packed structures, whereas focusing chains necessarily pass through many lattice sites.

[31] O. S. Oen and M. T. Robinson, Appl. Phys. Letters **2**, 83 (1963).

[32] J. R. Beeler, Jr., and D. G. Besco, in *Radiation Damage in Solids* (International Atomic Energy Agency, Vienna, 1962), p. 43; J. Phys. Soc. (Japan) **18**, Suppl. III, 159 (1963); Bull. Am. Phys. Soc. **8**, 339 (1963); J. Appl. Phys. **34**, 2873 (1963); D. G. Besco and J. R. Beeler, Jr., Bull. Am. Phys. Soc. **8**, 339 (1963).

[33] R. H. Silsbee, J. Appl. Phys. **28**, 1246 (1957); G. Leibfried, *ibid.* **31**, 117 (1960).

[34] M. L. Swanson, G. R. Piercy, and D. J. Mackinnon, Phys. Rev. Letters **9**, 418 (1962).

Finally, we close with a remark on terminology. Although we have not had occasion to do so in this communication, the need will likely arise to refer to a channeled atom (or trajectory) as a particle with a characteristic name. We suggest for this purpose the term *stenon*, from the Greek noun τα στενός, denoting a strait or a mountain pass.[35]

[35] H. G. Liddell and R. Scott, *Greek-English Lexicon* (Oxford University Press, London, 1940), p. 1638.

ACKNOWLEDGMENT

We are particularly grateful to J. A. Davies and G. R. Piercy of Atomic Energy of Canada Ltd., Chalk River, Ontario, for communicating much of their experimental data to us in advance of publication, for permission to reproduce Fig. 17, and for several stimulating and fruitful conversations.

It is a pleasure to acknowledge many valuable discussions with our colleagues C. Lehmann, G. Leibfried, and especially D. K. Holmes.

PHYSICAL REVIEW VOLUME 132, NUMBER 6 15 DECEMBER 1963

Spin-Wave Spectra of Yttrium and Gadolinium Iron Garnet*

A. Brooks Harris
Department of Physics, Duke University, Durham, North Carolina
(Received 13 May 1963)

The problem of deducing the values of the exchange integrals in yttrium and gadolinium iron garnet from measurements of the magnetization and the magnetic contribution to the specific heat at low temperatures is considered. For these garnets the spin-wave normal modes can be found by solving the semiclassical equations of motion which give rise to a set of n simultaneous linear equations, where n is the number of magnetically inequivalent ions in the unit cell. Expressions for the thermodynamic functions at low temperatures in terms of the frequencies of the normal modes are given assuming the validity of the spin-wave approximation. It is argued that the temperature variation of the frequency of these normal modes on the macroscopic properties can be completely accounted for without considering the zero point energy explicitly. Due to the size of the unit cell, the equations for the frequencies of the normal modes can only be solved numerically for general values of $\mathbf{k}$. Such solutions are obtained for $\mathbf{k}$ lying along a [111] direction for various values of the exchange integrals, and the thermodynamic functions corresponding to these choices of parameters are calculated. In the case of yttrium iron garnet, the value of D, the coefficient of a^2k^2 in the acoustic dispersion law, is reliably known and fixes one linear combination of J_{aa}, J_{ad}, and J_{dd}. By comparing our calculations with the magnetization data of Solt, it was established that $J_{aa}/J_{ad}=0.2$, but since the magnetization was not very sensitive to variations of the ratio J_{dd}/J_{ad} its value could not be estimated precisely. Taking $J_{dd}/J_{ad}=0.2$ gives $J_{aa}=J_{dd}=6.35$ cm^{-1} and $J_{ad}=31.8$ cm^{-1}. For GdIG the specific heat data below 20°K is not very much influenced by the exact values of the iron-iron exchange integrals which were taken to be those quoted above for yttrium iron garnet. Again one combination of J_{ac} and J_{dc} is known from the calorimetric determination of the single ion splitting. By comparing the specific heat data below 5°K with calculations for various values of J_{ac}/J_{dc} it was possible to determine J_{ac} and J_{dc} separately: $J_{dc}=7.00$ cm^{-1} and $J_{ac}=1.75$ cm^{-1}. These values are about 25% larger than what one would expect using the Weiss molecular field approximation.

I. INTRODUCTION

RECENTLY many investigations of the behavior of the series of iron garnet compounds have been made. Pauthenet[1] first interpreted their magnetic properties below the Néel point at 550°K using the Weiss molecular field (WMF) approximation. More recently it has been demonstrated[2–5] that at the lowest temperatures one must use the spin-wave approximation in many cases to interpret the thermal and magnetic properties of the iron garnets. The earliest calculations[3,4] gave a value of the excitation energy of the various normal modes (spin waves) for $\mathbf{k}=0$, where $\mathbf{k}$ is a vector of the first Brillouin zone. While this is often sufficient to describe the resonance behavior of the iron garnets, it would seem desirable to make more accurate calculations of the macroscopic properties which take into account the $\mathbf{k}$ dependence of the excitation energies. Tinkham[5] has made such a calculation for a simplified model of the interactions in ytterbium iron garnet (YbIG). He has shown that there are spin-wave modes whose energy is not very dependent on $\mathbf{k}$ and is roughly equal to the energy of the single ion splitting of the rare-earth ion in the WMF approximation, which can be determined calorimetrically.[6] Thus the physical picture of the magnetic behavior of the

* Work carried out with support of the U. S. Office of Naval Research under Contract Nonr 1811(12).
[1] R. Pauthenet, Ann. Phys. **3**, 424 (1958); J. Phys. Radium **20**, 388 (1959).
[2] H. Meyer and A. B. Harris, J. Appl. Phys. **31**, 49S (1960).
[3] R. L. Douglass, Phys. Rev. **120**, 1612 (1960).
[4] B. Dreyfus, J. Phys. Chem. Solids **23**, 287 (1962).
[5] M. Tinkham, Phys. Rev. **124**, 311 (1961).
[6] A. B. Harris and H. Meyer, Phys. Rev. **127**, 101 (1962).